Research Square

Preprints are preliminary reports that have not undergone peer review.
They should not be considered conclusive, used to inform clinical practice,
or referenced by the media as validated information.

Delay-Compensated Complementary Coordination of Grid-Forming and Grid-Following Energy Storage for Primary Frequency Regulation with an Identification-Based Frequency-Security Guard

Muzeeb Khan Patan

Muzeeb.Patan@utas.edu.om

University of Technology and Applied Sciences

Research Article

Keywords: Grid-forming converter, Grid-following converter, Energy storage, Primary frequency regulation, Virtual inertia, Islanding, Converter current limit

Posted Date: November 17th, 2026

DOI: https://doi.org/10.21203/rs.3.rs-11084433/v1

License: This work is licensed under a Creative Commons Attribution 4.0 International License.
Read Full License

Additional Declarations: No competing interests reported.

Delay-Compensated Complementary Coordination of Grid-Forming and Grid-Following Energy Storage for Primary Frequency Regulation with an Identification-Based Frequency-Security Guard

Muzeeb Khan Patan

Senior Lecturer, Electrical, Electronics, and Computer Engineering (EECE) Unit

Department of Engineering and Technology, University of Technology and Applied Sciences, Muscat, Sultanate of Oman.

Corresponding Author: Muzeeb Khan Patan**, Email:** Muzeeb.Patan@utas.edu.om

Abstract

Converter-interfaced energy storage now carries a growing share of primary frequency regulation, but its two control modes fail in opposite ways: grid-following (GFL) units can be rated large yet act through a phase-locked loop and a measurement delay, while grid-forming (GFM) units act at once but are small and tightly current limited. This paper proposes a predictive complementary split with a robust frequency-security guard (PCS-RG). When grid connected, the GFM unit supplies virtual inertia and a wash-out droop while the GFL unit applies an event-triggered, front-loaded droop to a frequency predicted from the rate of change of frequency (RoCoF), which offsets the GFL delay without forecasting the nadir. After islanding the GFM unit follows an energy-aware trajectory of inertia, transient droop and ramped steady droop, and a guard identifies the power imbalance and the governor droop online, raising the droop only when the steady-state limit is at risk; if synchronous machines remain, the GFL unit re-locks and carries that droop. On a three-area average-system-frequency model the scheme lowers the nadir by 9.6% at unchanged state of charge, keeps it 33% lower at 300 to 400 ms of delay, cuts islanded RoCoF by 30% and removes every steady-state violation in 120 randomised islands, where a deviation-scheduled benchmark violates in 48% of cases. A validation on the IEEE 10-machine 39-bus system with machine dynamics and explicit converter current limits gives the benchmark nadir with 41% less GFM peak power after a generator trip and, in a 15-bus island with a 548 MW deficit, a 0.161 Hz nadir and a 0.068 Hz settling deviation where the benchmark saturates its converter, exhausts it after 15 s and settles outside a 0.12 Hz limit.

Keywords Grid-forming converter · Grid-following converter · Energy storage · Primary frequency regulation · Virtual inertia · Islanding · Converter current limit

1 Introduction

Synchronous generators are being displaced by converter-interfaced sources, and the kinetic energy that once slowed frequency excursions is shrinking with them [1-3]. After a large power imbalance, a low-inertia system shows a faster rate of change of frequency (RoCoF) and a deeper nadir. Reduced-order frequency response models [4] and integration-limit studies [5] show that these two indices, rather than the final steady-state deviation, now often set how much inverter-based generation a system can accept.

Energy storage (ES) can deliver fast primary frequency regulation (PFR). Oudalov et al. sized a battery system for primary frequency control while keeping its state of charge (SOC) within bounds [6], and the sizing question has since been posed for hybrid battery and supercapacitor plants whose two media are matched to different parts of the frequency spectrum [7]. Storage has also been embedded in automatic generation control for deregulated areas [8], and photovoltaic plants have been given frequency support functions of their own [9]. Virtual inertia control has been applied to interconnected systems with high renewable penetration [10].

The converter control mode matters as much as the storage behind it. Grid-forming (GFM) converters set their own voltage phasor and behave like a voltage source behind an impedance, so they supply inertial power without waiting for a frequency measurement and can energise an island [11-13]. The virtual synchronous generator (VSG) is the most common GFM scheme; it damps oscillations of distributed generators [14], its parameters have been tuned by population-based search for inverter-interfaced distributed generation [15], and adaptive inertia laws built on oscillator control have been proposed to trade damping against overshoot during the swing [16]. Because a GFM converter has to hold its voltage while its current is strictly limited, its transient stability under fault current has also received attention [17], as has its voltage support capability in photovoltaic plants [18]. Grid-following (GFL) converters, in contrast, inject current synchronised by a phase-locked loop (PLL). Their frequency estimate is delayed and filtered, their small-signal behaviour differs from that of a GFM unit at every frequency of interest [19], and their synchronisation can become fragile in weak grids [20]. This paper considers an area in which a large GFL storage unit and a smaller GFM storage unit operate together, which is the usual outcome when a legacy plant is retrofitted alongside a new grid-forming installation.

Coordinating the two types raises three problems that existing schemes do not solve together. First, the GFL delay. Sharing rules that divide power by fixed ratios, or by the ratio of the present deviation to an expected nadir, must either accept the delay or forecast the nadir, and the nadir is not known when the event starts. SOC-adaptive droop laws manage the energy of each unit [21], and two-stage balancing schemes equalise the SOC of distributed units [22], but neither addresses timing. Second, delays in frequency control loops erode stability margins [23], and a gain schedule that switches at the nadir makes those margins hard to certify because the loop is no longer time invariant. Third, after

islanding the storage coefficients are usually sized once from static frequency limits. That sizing depends on the exact disturbance, inertia and governor droop of the island. Estimators for the time of a disturbance and for system inertia exist [24], and RoCoF-based relays detect the islanding event itself [25], but the author is not aware of their use for correcting a storage droop while the islanding event is still in progress.

This paper proposes PCS-RG, a predictive complementary split with a robust frequency-security guard. Its contributions are as follows. (i) A nadir-free allocation between GFM and GFL storage, in which the GFM unit provides inertia and a wash-out droop and the GFL unit applies an event-triggered, front-loaded droop to a delay-compensated frequency. The controller is linear and time invariant between events, so its delay margin can be computed directly. (ii) An energy-balance argument that shows which PFR indices can be improved together for a given storage energy; combined with differential evolution tuning [26] it guides where the storage energy is spent in time. (iii) An islanded frequency-security (FS) trajectory with a closed-loop guard that identifies the imbalance and the effective governor droop online and raises the steady droop only when the steady-state limit would otherwise be violated. (iv) An island-aware mode in which the GFL unit re-locks to an island that still contains synchronous machines, which preserves the GFM energy for later contingencies. (v) A validation of all four items on the IEEE 10-machine 39-bus system [27], [28] with a network solution, machine and governor dynamics and an explicit converter current limit [29], which is where the ranking between the proposed scheme and a strong benchmark is decided.

Section 2 gives the system model and the frequency-security indices. Section 3 describes PCS-RG and Section 4 analyses its small-signal stability. Section 5 reports results on an average-system-frequency model, Section 6 reports the 39-bus validation, and Section 7 concludes.

2 System Model and Frequency-Security Indices

2.1 Multi-Area Frequency Dynamics

Each control area i is represented by an aggregated swing equation, as in reduced-order frequency response studies [4]:

$$2H_i \frac{d\Delta f_i}{dt} = \Delta P_{G,i} + \Delta P_{ES,i} - \Delta P_{T,i} - \Delta P_{L,i} - D_i \Delta f_i \quad (1)$$

$$\Delta P_{T,i} = \Sigma_j \frac{2\pi T_{ij}}{s} (\Delta f_i - \Delta f_j) \quad (2)$$

where H_i and D_i are the inertia constant and the load damping of area i, and T_{ij} is the tie-line synchronising coefficient between areas i and j. The thermal units in each area have a governor and a reheat turbine:

$$\Delta P_{G,i} = -\frac{K_{G,i}}{1+sT_G} R_t(s) \Delta f_i,$$

$$R_t(s) = \frac{F_{HP}}{1+sT_{CH}} + \frac{F_{IP}}{(1+sT_{CH})(1+sT_{RH})} + \frac{F_{LP}}{(1+sT_{CH})(1+sT_{RH})(1+sT_{CO})} \quad (3)$$

2.2 Storage Units

Both storage units sit in area 1. The GFL unit follows a power command u_{GFL} through its PLL and measurement delay τ and a current-loop lag T_E. The GFM unit follows its droop command through the same lag, but its inertial power acts without delay because it comes from the internal frequency dynamics of the converter [14], [16]:

$$P_{GFL}(s) = \frac{e^{-\tau s}}{1+sT_E} u_{GFL}(s),$$
$$P_{GFM}(s) = \frac{u_{GFM}(s)}{1+sT_E} - K_I s\Delta f(s) \quad (4)$$

The SOC S of each unit is integrated from its power with charge or discharge efficiency η and normalised energy capacity E_n in p.u.·s. Every gain is multiplied by a logistic factor g(S) that is close to unity in the normal SOC band and falls to zero at S_{min} or S_{max}:

$$\frac{dS}{dt} = -\frac{\eta^{\pm 1} P}{E_n}, \quad x = \frac{S - S_{min}}{S_{max} - S_{min}},$$
$$g(S) = \frac{P_0 e^{2nx}}{1 + P_0(e^{2nx} - 1)} \quad (5)$$

Equation (5) is written for discharge; for charge, x is measured from S_{max}. The factor is normalised to unity at S = 0.5. This is the same mechanism used in SOC-adaptive droop schemes [21], [22], applied here to both units.

2.3 Frequency-Security Indices and the Energy Balance

Frequency security is assessed with three limits: $|\Delta f|_{max} \leq 0.1$ Hz, $|\text{RoCoF}|_{max} \leq 0.2$ Hz/s and $|\Delta f_{ss}| \leq 0.033$ Hz, that is 2×10^{-3} p.u., 4×10^{-3} p.u./s and 6.6×10^{-4} p.u. on a 50 Hz base. For a single area with total steady droop K_{ss} from storage, the steady-state deviation is

$$|\Delta f_{ss}| = \frac{\Delta P_L}{D + K_G + K_{ss}} \quad (6)$$

Integrating (1) over a window $[t_0, t_1]$ after a step ΔP_L gives the energy delivered by the storage:

$$\int P_{ES} dt = \Delta P_L(t_1 - t_0) - \int \Delta P_G dt - D\int |\Delta f| dt - 2H|\Delta f(t_1)| \quad (7)$$

Because ΔP_G is a lagged linear function of Δf, any controller that lowers $\int|\Delta f|dt$ also lowers the governor contribution and must therefore deliver more storage energy. For a fixed plant the average deviation and the storage energy cannot both be reduced. What a controller can change is when the energy is spent. Energy delivered in the first second acts mainly on RoCoF and on the nadir, while energy delivered later acts mainly on the average deviation. PCS-RG is built around this observation, and Section 5.2 reports the trade-off that it implies rather than hiding it.

3 Proposed PCS-RG Controller

Figure 1 shows the controller. It has a grid-connected part, which runs continuously, and an islanded part, which is activated by the breaker status. Neither part needs a forecast of the nadir.

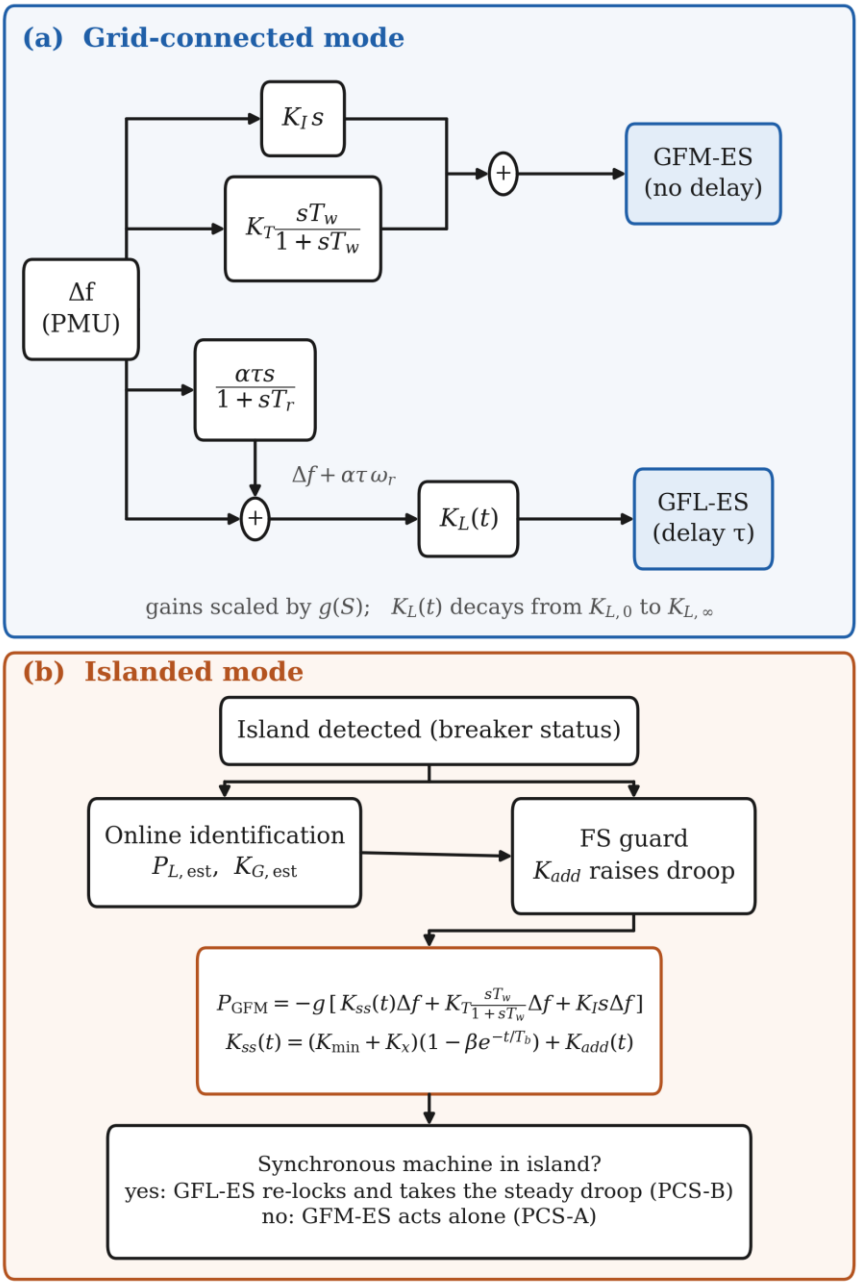


Fig. 1 Structure of the proposed PCS-RG controller. a Grid-connected mode. b Islanded mode

3.1 Grid-Connected Mode

The GFM unit provides full virtual inertia and a droop that washes out with time constant T_w:

$$u_{GFM} = -g(S_{GFM})K_T \frac{sT_w}{1+sT_w}\Delta f,$$
$$inertia\ gain: g(S_{GFM})K_I \quad (8)$$

Its output therefore covers the first few hundred milliseconds, when the GFL unit has not yet reacted, and then fades without a latch. The GFL unit applies its droop to a frequency predicted one delay ahead from the filtered RoCoF:

$$u_{GFL} = -g(S_{GFL})K_L(t)[\Delta f + \alpha\tau\omega_r],$$
$$\omega_r = \frac{s}{1+sT_r}\Delta f \tag{9}$$

$$K_L(t) = K_{L,\infty} + (K_{L,0} - K_{L,\infty})e^{-(t-t_d)/T_L} \tag{10}$$

Here $\alpha \in [0, 1.5]$ sets how much of the delay τ is compensated, $T_r = 20$ ms filters the RoCoF, and t_d is the instant at which $|\Delta f|$ first exceeds 10^{-5} p.u. The front-loaded gain $K_{L,0} > K_{L,\infty}$ spends GFL energy early, where (7) shows it has the most effect on the nadir. All gains respect the unit limits $0 \le K_L, K_T \le K^D_{max}$ and $0 \le K_I \le K^I_{max}$. Unlike a deviation-scheduled split, (8) to (10) contain no division by an expected nadir and no switching at the extremum, so the loop stays linear and time invariant between events.

3.2 Islanded Mode: Energy-Aware Frequency-Security Trajectory

When the breaker status shows that area 1 has separated, the GFM unit switches to

$$u_{GFM} = -g[K_{ss}(t)\Delta f + K_T\frac{sT_w}{1+sT_w}\Delta f],$$
$$K_{ss}(t) = (K_{min} + K_x)(1 - \beta e^{-t/T_b}) + K_{add}(t) \tag{11}$$

with the virtual inertia K_I kept active. The minimum steady droop follows from (6) and the pre-event estimates, $K_{min} = \Delta P_{L,est}/\Delta f_{ss}^{lim} - K_{G,est} - D_{est}$. The ramp ($\beta$, T_b) postpones part of the steady droop while the reheat turbines are still rising, and the energy saved pays for the inertia and the transient droop, which act on RoCoF and on the nadir.

3.3 Online Identification and the Frequency-Security Guard

A one-shot K_{min} is exact only if ΔP_L, K_G and D are known exactly. The guard replaces these assumptions with measurements. The imbalance is estimated from the measured governor and storage power through (1) and low-pass filtered with a 1 s time constant. After the nadir $d\Delta f/dt$ is small, so an error in H_{est} has little influence:

$$\Delta P_{L,est} = -[P_G + P_{ES} - D_{est}\Delta f - 2H_{est}\frac{d\Delta f}{dt}] \tag{12}$$

The effective governor droop is identified by least squares, regressing the measured governor power on the response z of the nominal turbine model (3) driven by the measured frequency, in the spirit of the transient-data estimators in [24]:

$$K_{G,est} = \frac{\int(-P_G)z\,dt}{\int z^2 dt}, \quad z = \frac{R_t(s)}{1+sT_G}\Delta f \tag{13}$$

The required droop is recomputed with a margin $\rho = 0.98$, and the extra droop follows it through a first-order filter with $\gamma = 4$ s^{-1} that can only add droop, never remove it:

$$K_{req} = \frac{|\Delta P_{L,est}|}{\rho \Delta f_{ss}^{lim}} - K_{G,est} - D_{est},$$

$$\frac{dK_{add}}{dt} = \gamma[max(K_{req} - K_{min} - K_x, 0) - K_{add}] \quad (14)$$

3.4 GFL Re-Lock in Islands That Retain Synchronous Machines

A GFL unit cannot form an island, but it can operate in one that already has a voltage reference. If the separated area still contains synchronous generators, or the GFM unit, and the short-circuit ratio at the GFL bus is adequate [20], the GFL unit is allowed to re-lock. Its output is held at zero for T_{relock} = 250 ms, after which it carries the steady droop, using at least its nominal grid-connected coefficient K^D_0 = 25:

$$u_{GFL} = -g(S_{GFL})max(K_{ss}, K_0^D)(\Delta f + 0.5\tau\omega_r), \quad t \geq t_{isl} + T_{relock} \quad (15)$$

The GFM unit then keeps only inertia and transient droop. This variant is called PCS-B; the GFM-only variant of Section 3.2 is called PCS-A. Islanding itself is taken from the breaker status, which a RoCoF-based relay of the kind described in [25] can supplement where breaker telemetry is not available.

3.5 Parameter Tuning

The parameter vectors θ_c = [K_I, K_T, T_w, $K_{L,0}$, $K_{L,\infty}$, T_L, α] and θ_i = [K_x, K_T, T_w, K_I, β, T_b] were tuned offline by differential evolution [26] on the nominal step events. Each index M_j, namely the nadir, the average deviation, RoCoF and the minimum SOC of each unit, was divided by its value under benchmark B4 of Section 5.1, giving ρ_j, and the objective

$$J = 0.5\rho_{nadir} + 0.3\rho_{RoCoF} + 0.2\rho_{ave} + 20\Sigma max(\rho_j - 1,0) \quad (16)$$

was minimised. The penalty term discourages any index from becoming worse than the benchmark. A second, balanced preset minimises the largest ρ_j instead. Table 1 lists the tuned values.

Table 1 Tuned PCS-RG parameters

Mode	Values
Grid-connected (FS priority)	K_I = 5.00, K_T = 0.43, T_w = 0.955 s, $K_{L,0}$ = 30.59, $K_{L,\infty}$ = 22.09, T_L = 1.218 s, α = 0.638
Grid-connected (balanced)	K_I = 4.79, K_T = 1.25, T_w = 0.133 s, $K_{L,0}$ = 25.97, $K_{L,\infty}$ = 19.80, T_L = 9.61 s, α = 0.461
Islanded (PCS-A and PCS-B)	K_x = 1.91, K_T = 2.58, T_w = 0.508 s, K_I = 4.28, β = 0.31, T_b = 13.1 s
Guard and re-lock	ρ = 0.98, γ = 4 s^{-1}, imbalance filter 1 s, T_{relock} = 0.25 s, K^D_0 = 25

4 Small-Signal Stability

Between events PCS-RG is linear, so its stability can be checked by eigenvalue analysis. The three-area model of (1) to (4) with the controller (8) to (10) was linearised, the delay $e^{-\tau s}$ was replaced by a fourth-order Pade approximation, and K_L was frozen at $K_{L,0}$, its largest value, and at $K_{L,\infty}$. Table 2

gives the delay at which the first eigenvalue crosses into the right half plane and the minimum damping ratio ζ_{min} of the oscillatory modes. Figure 3b shows ζ_{min} against τ.

Table 2 Delay margin and minimum damping ratio of the linearised three-area model

Controller	Delay margin (s)	ζ_{min} at τ = 0.1 s	ζ_{min} at τ = 0.3 s
PCS-RG, $K_L = K_{L,0}$	0.570	0.245	0.204
PCS-RG, $K_L = K_{L,\infty}$	0.740	0.249	0.248
PCS-RG without GFM inertia	0.385	0.244	0.121
Same GFL gain, $\alpha = 0$	0.415	0.243	0.159
B1 (GFL droop and inertia)	0.570	0.213	0.183

With the predictor removed, the same GFL gain loses 27% of its delay margin, 0.415 s against 0.570 s, and its damping at 300 ms falls from 0.204 to 0.159. Removing the GFM inertia costs even more, 0.385 s. PCS-RG runs a GFL gain 22% higher than benchmark B1, yet it keeps the same margin and has better damping up to 300 ms. The GFM inertia and the predictor together recover most of the phase that the delay removes, which is consistent with the delay-dependent bounds reported for load frequency control loops [23].

5 Results on the Average-System-Frequency Model

5.1 Test System and Benchmarks

The test system has three areas. Area 1 has H = 5 s, D = 1 and K_G = 20 on its own base; areas 2 and 3 are twice as large, with H = 10 s, D = 2 and K_G = 40. The tie-line coefficients are T_{12} = 1.6, T_{13} = 1.1 and T_{23} = 0.8. The turbine data are T_G = 0.2 s, T_{CH} = 0.3 s, T_{RH} = 7 s, T_{CO} = 0.5 s and $F_{HP}/F_{IP}/F_{LP}$ = 0.3/0.3/0.4. Both storage units are in area 1, with T_E = 10 ms, τ = 100 ms for the GFL unit, rated power 0.08 p.u., η = 0.95, S_{min} = 0.1, S_{max} = 0.9 and an initial SOC of 0.5. The energy capacities are 3.40 p.u.·s for the GFL unit and 0.68 p.u.·s for the GFM unit, about 42 s and 8.5 s at rated power. These are short-duration units, chosen deliberately so that energy limits become visible within the PFR horizon. The coefficient limits are K^D_{max} = 50 and K^I_{max} = 5 per unit. The disturbance is a 0.02 p.u. load step in area 1 at t = 2 s. For islanded tests area 1 is studied alone on its own base. The model is integrated with a fixed step of 0.5 ms.

Four benchmarks are compared (Table 3). B4 is a strong deviation-scheduled benchmark constructed for this study. It shares power in proportion to $|\Delta f|/\Delta f_{max}$, hands over completely to the GFL unit at the nadir, and in the island sets its droop and inertia once from the limits in (6) and from the RoCoF limit. To favour B4, it is given the exact nadir of its own response as Δf_{max}, which no real implementation could know in advance.

Table 3 Benchmark strategies

Name	Grid-connected	Islanded
B1	GFL only, $K^D = 25$, $K^I = 5$, acting through the delay	GFL unavailable
B2	GFM only, $K^D = 25$, $K^I = 5$	GFM, $K^D = 25$, $K^I = 10$
B3	Equal fixed sharing of the B1 and B2 gains	As B2
B4	Deviation-scheduled handover, GFM first and GFL after the nadir	GFM, one-shot minimum K^D and K^I from the FS limits

5.2 Grid-Connected Step Response

Table 4 and Fig. 2 compare the responses. PCS-RG in its FS-priority setting gives the lowest nadir of all strategies, 9.6% below B4, with the same RoCoF and the same minimum SOC for both units. B1, B2 and B3 reach nadirs about 4% below B4, but B2 and B3 draw heavily on the small GFM unit, whose minimum SOC falls to 0.41 and 0.46, and B1 and B3 leave RoCoF higher. The GFM power under PCS-RG in Fig. 2c delivers almost the same energy as under B4, but fades smoothly rather than being cut at the nadir. The GFL unit responds earlier, because of the predictor and because its share is not held back until the nadir.

Table 4 Grid-connected indices over 2 to 10 s. Deviations in 10^{-4} p.u., RoCoF in 10^{-3} p.u./s

Strategy	$\lvert\Delta f\rvert_{max}$	$\lvert\Delta f\rvert_{ave}$	RoCoF	$S_{GFL,min}$	$S_{GFM,min}$
B1	4.969	2.791	2.000	0.4826	0.5000
B2	4.928	2.790	1.333	0.5000	0.4122
B3	4.954	2.790	1.600	0.4913	0.4561
B4	5.168	2.792	1.336	0.4833	0.4961
PCS-RG (FS priority)	4.674	2.851	1.333	0.4833	0.4962
PCS-RG (balanced)	4.954	2.828	1.352	0.4831	0.4962

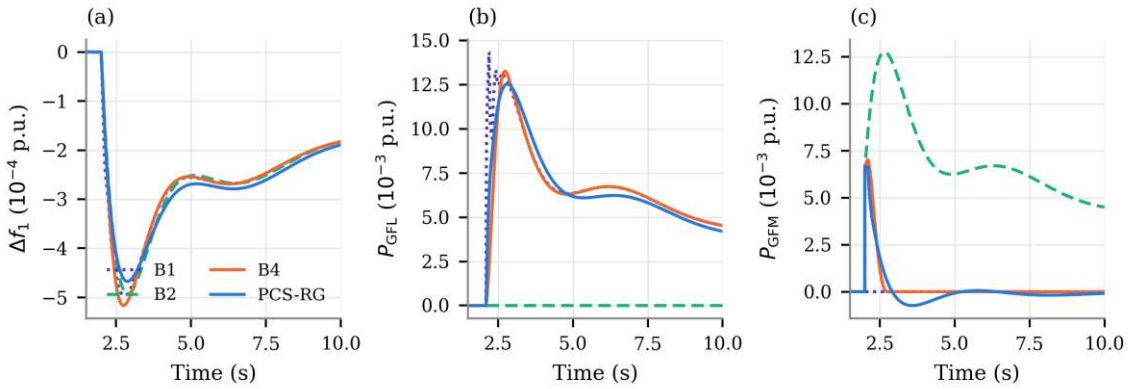


Fig. 2 Grid-connected response to a 0.02 p.u. load step in area 1. a Frequency deviation of area 1. b GFL-ES power. c GFM-ES power

The price is a 2.1% higher average deviation, 6×10^{-6} p.u. or about 0.3 mHz. Equation (7) explains why this cannot be avoided at equal storage energy: the controller moves energy toward the first seconds, where it lowers the nadir, and away from the later recovery, where it would lower the average. The balanced preset trades the other way, with the nadir 4.1% lower, the average deviation 1.3% higher

and RoCoF 1.2% higher. A search over all tuning parameters found no setting that beats B4 on all five indices at once; the best largest ratio was about 1.01.

5.3 Robustness to the GFL Delay

Figure 3a repeats the step with GFL delays of 100 to 400 ms. The nadir under B4 grows from 5.17×10^{-4} p.u. at 100 ms to 5.90, 7.21 and 8.42×10^{-4} p.u. at 200, 300 and 400 ms, because the handover at the nadir passes the task to a unit that reacts ever later. Under PCS-RG the nadir is 4.67, 4.64, 4.81 and 5.54×10^{-4} p.u., which is 21.4%, 33.3% and 34.1% lower than B4 at 200, 300 and 400 ms, while RoCoF stays at 1.333×10^{-3} p.u./s.

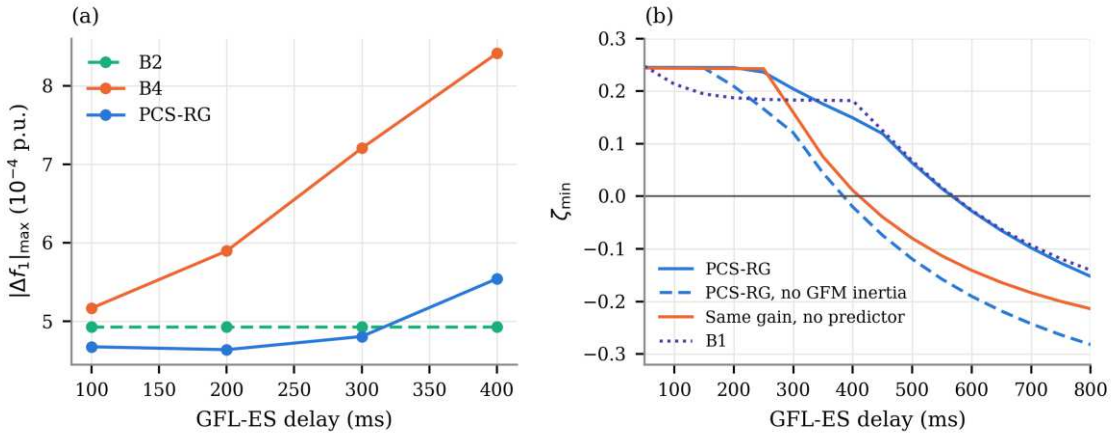


Fig. 3 Effect of the GFL-ES measurement delay. a Nadir against delay. b Minimum damping ratio of the linearised model

B4 also depends on its nadir forecast. With a forecast of 1.5 or 3 times the true value its nadir rises to 5.44 or 5.75×10^{-4} p.u. With half the true value its nadir improves to 5.02×10^{-4} p.u., but RoCoF rises to 1.546×10^{-3} p.u./s because the GFM inertia is withdrawn too early. PCS-RG has no such input.

5.4 Islanded Operation

Table 5 and Fig. 4 show the island alone after a 0.02 p.u. step. B4 sets $K^D = 9.3$ so that Δf_{ss} lands exactly on its limit, and uses no inertia because the predicted RoCoF is within its limit. PCS-A keeps the GFL unit out, as B4 does, and matches B4 in minimum SOC and average deviation while lowering RoCoF by 30.0% and the nadir by 2.2%. When the GFL unit is allowed to re-lock, in PCS-B, the nadir falls by 49.2% and the average deviation by 39.5%, close to the GFM-heavy B2, while the minimum GFM SOC rises from 0.35 to 0.49. The GFL unit spends 0.05 of its SOC to achieve this.

Table 5 Islanded indices over 2 to 15 s. Deviations in 10^{-3} p.u., RoCoF in 10^{-3} p.u./s

Strategy	$\|\Delta f\|_{max}$	$\|\Delta f\|_{ave}$	RoCoF	$S_{GFM,min}$	$S_{GFL,min}$
No storage	2.415	1.306	2.000	-	-
B2 and B3	0.603	0.509	1.000	0.2463	-
B4	1.207	0.828	2.000	0.3451	-
PCS-A	1.181	0.829	1.401	0.3454	-
PCS-B	0.613	0.501	1.401	0.4948	0.4498

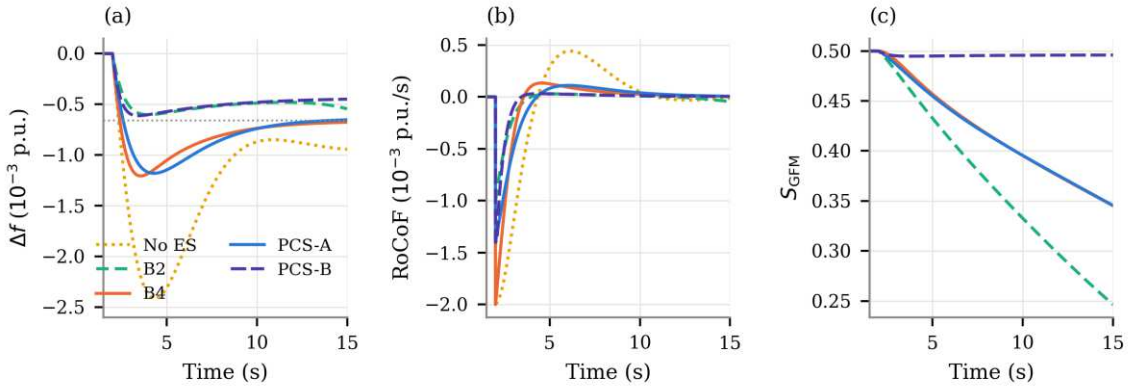


Fig. 4 Islanded response to a 0.02 p.u. load step. a Frequency deviation, with the steady-state limit dotted. b RoCoF. c GFM-ES state of charge

5.5 Grid-Connected to Islanded Transition

In this test a 0.02 p.u. step occurs at 5 s while the system is connected, and area 1 separates at 15 s with a further 0.012 p.u. step. The cumulative island imbalance of 0.032 p.u. gives a minimum steady droop of 27.5. Table 6 and Fig. 5 show the results. Under every GFM-only strategy the GFM SOC approaches 0.25 after about 22 s. The logistic factor then reduces the gains and the frequency deteriorates again, a direct consequence of the short-duration GFM unit. PCS-A delays this: its island nadir is 14.7% lower than B4, its RoCoF 28.8% lower and its final SOC 6.4% higher, although its average deviation is 4.8% higher. PCS-B removes the problem: the island nadir is 37.0% lower and the GFM unit stays at SOC 0.49, ready for a further contingency.

Table 6 Transition test. Connected window 5 to 15 s in 10^{-4} p.u., island window 15 to 25 s in 10^{-3} p.u.

Strategy	Conn. $\|\Delta f\|_{max}$	Isl. $\|\Delta f\|_{max}$	Isl. $\|\Delta f\|_{ave}$	Isl. RoCoF	Isl. $S_{GFM,min}$
B3	4.953	1.762	1.002	1.207	0.1780
B4	5.167	1.378	0.851	2.410	0.1988
PCS-A	4.674	1.176	0.892	1.717	0.2115
PCS-B	4.674	0.868	0.750	1.917	0.4926

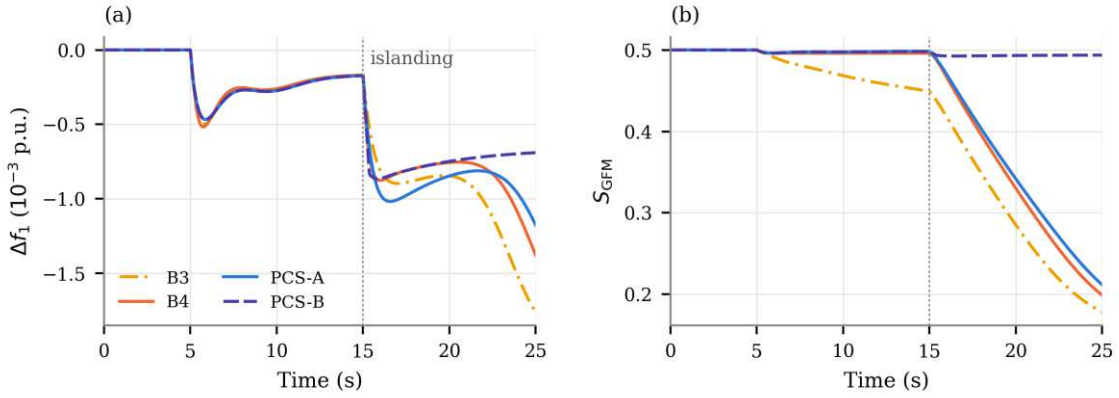


Fig. 5 Transition test with islanding at 15 s. a Frequency deviation of area 1. b GFM-ES state of charge

5.6 Monte Carlo Test of the Guard

The islanded step was repeated for 120 random islands with H ~ U[4, 6] s, K_G ~ U[16, 24], D ~ U[0.5, 1.5], T_{RH} ~ U[5, 9] s and a true disturbance of 0.02·U[0.85, 1.15] p.u. Every controller received the same nominal estimates. The steady-state deviation was evaluated from (6) with the final droop of each controller. Because B4 is sized exactly at the limit, about half of the estimation errors push it over, as Table 7 and Fig. 6 show. The guard in PCS-A removes every violation, at the cost of a 0.005 lower mean SOC spent only in the cases that needed more droop. PCS-B stays well inside the limit.

Table 7 Monte Carlo results for 120 randomised islands

Index	B4	PCS-A	PCS-B
Δf_{ss} limit violations	48.3%	0%	0%
Δf_{ss}/limit, mean / worst	1.007 / 1.293	0.918 / 0.982	0.662 / 0.812
$\lvert\Delta f\rvert_{max}$ (10^{-3} p.u.), mean / worst	1.213 / 1.457	1.185 / 1.428	0.615 / 0.716
RoCoF (10^{-3} p.u./s), worst	2.719	1.774	1.774
$S_{GFM,min}$, mean / worst	0.345 / 0.301	0.339 / 0.264	0.495 / 0.494

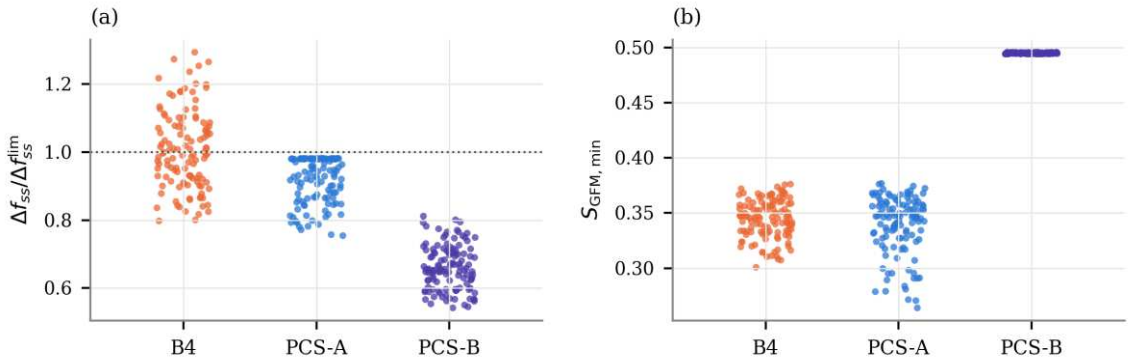


Fig. 6 Monte Carlo results for 120 randomised islands. a Steady-state deviation relative to its limit. b Minimum GFM-ES state of charge

6 Validation on the IEEE 39-Bus System with Converter Current Limits

6.1 Why a Network Model with Current Limits Is Required

The model of Section 2 aggregates each area into one bus and represents each storage unit as a power injection that is bounded only by its rating and its SOC. Three of the claims made above are sensitive to what that abstraction leaves out. First, a converter is a current source with a hard magnitude limit, and the limit binds exactly when the frequency excursion is largest and the bus voltage is depressed [17], [29]. Second, a short-duration GFM unit can run its energy down inside the PFR horizon; the logistic factor of (5) represents the derating but not what happens to a weak island when its only grid-forming source stops supporting it. Third, the GFL re-lock of Section 3.4 assumes that the island retains a firm voltage reference, which is a network property and cannot be asserted in a single-bus model.

These omissions do not merely widen an error bar. They can reverse a ranking. A benchmark whose advantage comes from commanding a large GFM power is unaffected in an unconstrained model and is clipped in a limited one, so a scheme that reaches the same frequency performance with a smaller peak power moves from being equivalent to being strictly better. A validation on a recognised test system with a network solution, machine and governor dynamics and an explicit current limit is therefore not an optional addition to this study. It is the test that decides whether the islanded conclusions of Section 5 survive, and it is reported here in full, including the case in which the proposed scheme does not win.

6.2 Model

The IEEE 10-machine 39-bus New England system [27] is used, with network and power-flow data taken from the widely used MATPOWER case file [28] on a 100 MVA base and a total load of 6254 MW. Each machine is represented classically behind its transient reactance, with inertia constants referred to the system base from the public GENROU records of this system, 782.7 s in total. Every machine carries a TGOV1 governor with $R = 0.05$, $T_1 = 0.4$ s, $T_2 = 1.5$ s and $T_3 = 5$ s on a 1000 MVA machine base. Loads are constant impedance and are folded into the bus admittance matrix, which is rebuilt whenever a branch opens. Connected components of the network are tracked at every step, and a centre-of-inertia frequency is formed separately for each island. The differential equations are integrated with a fixed step of 2 ms.

The storage units are placed at load buses. The GFM unit is at bus 20, rated 150 MW with 1.25 MWh of usable energy, and the GFL unit is at bus 16, rated 300 MW with 5 MWh and a measurement delay of 100 ms. Both are injected as current sources. The commanded current is $I = (P/V)^*$, and its magnitude is clipped at the value corresponding to rated apparent power at nominal voltage, which is the elementary form of the current-limiting problem studied for grid-forming converters in [29]. A unit whose SOC falls to 0.05 stops injecting. The controllers receive a washed-out bus frequency and a filtered RoCoF rather than an ideal derivative, so that the predictor of (9) is exercised on a realistic signal. Table 8 collects the data.

Table 8 IEEE 39-bus validation model and converter data

Item	Value
Network and power flow	IEEE 10-machine 39-bus (New England); MATPOWER case39 data, 100 MVA base, 6254 MW load
Machines	Classical model behind x'_d; inertia from the public GENROU records, 782.7 s on the system base
Governors	TGOV1 on every machine: R = 0.05, T_1 = 0.4 s, T_2 = 1.5 s, T_3 = 5 s (1000 MVA machine base)
Loads	Constant impedance, folded into the bus admittance matrix, which is rebuilt when a branch opens
GFM-ES	Bus 20; 150 MW rating; 1.25 MWh usable energy; no measurement delay
GFL-ES	Bus 16; 300 MW rating; 5 MWh usable energy; measurement delay τ = 100 ms
Converter limit	Current magnitude clipped at rated apparent power; injection stops when the SOC reaches 0.05
Signals and integration	Washed-out bus frequency and filtered RoCoF; fixed step 2 ms; per-island centre-of-inertia frequency
Events	Trip of the 650 MW machine at bus 32; or opening of branches 3-18, 14-15 and 26-27 with a 300 MW load step at bus 20

Two events are studied. In the interconnected case the 650 MW machine at bus 32 is tripped at t = 1 s. In the islanding case the three branches 3-18, 14-15 and 26-27 are opened at t = 1 s, which separates a 15-bus island containing buses 15 to 24, 27 and the four machines at buses 33 to 36. That island carries 2598 MW of load against 2350 MW of local generation, an initial deficit of 248 MW, and a further 300 MW load step is applied at bus 20 at the same instant. The total deficit of 548 MW is 21% of the island load. The island inertia is 115.8 s on the system base, which is 4.46 s on the island load base, and the aggregate governor droop is 800 p.u. With a steady-state limit of 0.12 Hz, (6) gives K_{min} = 1939.5 for the islanded design. Both storage units lie inside the island, so the re-lock condition of Section 3.4 is satisfied and PCS-B is admissible.

6.3 Interconnected Contingency

The upper half of Table 9 gives the results for the generator trip. Without storage the centre-of-inertia frequency falls 0.239 Hz. B4 reaches 0.198 Hz and PCS-RG 0.201 Hz, so the benchmark is 1.1% better on the nadir and the two are effectively tied. This is the expected outcome and it is stated plainly: in a large interconnected system, 450 MW of storage against 6254 MW of load and 782.7 s of inertia cannot separate two well-tuned controllers on the nadir, and any paper that claims a large margin in this case should be read with suspicion.

The difference lies in how the two schemes buy that nadir. B4 commands a GFM peak of 42.1 MW and a GFL peak of 98.5 MW; PCS-RG commands 24.6 MW and 76.1 MW, which is 41.5% and 22.7% less. It also ends with more energy in both units, with minimum SOC 0.490 and 0.457 against 0.483 and 0.448 for the benchmark. Neither scheme reaches its current limit here. The practical reading is that PCS-RG achieves the same frequency performance with a smaller converter duty, which is a sizing argument rather than a frequency argument, and it becomes a frequency argument as soon as the limit binds.

Table 9 IEEE 39-bus results. Nadir and settling deviation of the centre-of-inertia frequency; "In limit" is the fraction of the window in which the GFM-ES current is clipped

Case and strategy	Nadir (Hz)	Δf_{end} (Hz)	RoCoF (Hz/s)	P_{GFM} (MW)	P_{GFL} (MW)	$S_{GFM,min}$	In limit (%)
Trip: no storage	0.239	0.104	0.154	-	-	-	-
Trip: B4	0.198	0.095	0.147	42.1	98.5	0.483	0.0
Trip: PCS-RG	0.201	0.098	0.145	24.6	76.1	0.490	0.0
Island: no storage	0.380	0.131	0.414	-	-	-	-
Island: B4	0.245	0.132	0.269	141.5	0.0	0.050	49.2
Island: PCS-A	0.246	0.132	0.275	141.5	0.0	0.050	48.8
Island: PCS-B	0.161	0.068	0.304	111.7	298.7	0.495	3.7

6.4 Islanding with a Large Deficit

The lower half of Table 9 and Fig. 7 report the islanding case, where the limit does bind. Without storage the island reaches 0.380 Hz and settles at 0.131 Hz, outside the steady-state limit. B4 and PCS-A behave almost identically: both hold their GFM converter at the current limit for about half of the 30 s window, 49.2% and 48.8% of the samples, both drive the GFM SOC to its 0.05 floor after roughly 15 s, and both then lose their only fast source. Figure 7a shows the consequence, a second dip to 0.22 Hz at the moment the GFM unit stops, followed by a settling point of 0.132 Hz, which is outside the 0.12 Hz limit. The one-shot island design of B4 and the FS trajectory of PCS-A are both correct as droop calculations; neither can help once the converter has no energy and no headroom left.

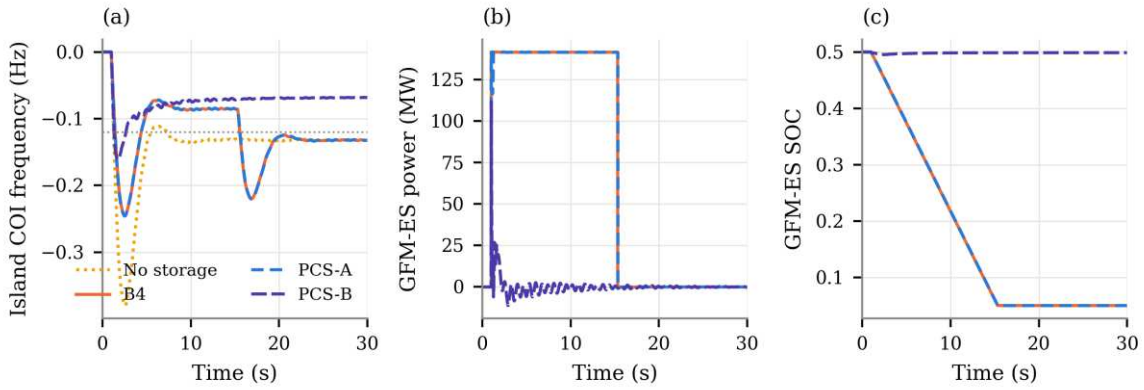


Fig. 7 IEEE 39-bus islanding case with a 548 MW deficit. a Island centre-of-inertia frequency, with the 0.12 Hz steady-state limit dotted. b GFM-ES power. c GFM-ES state of charge

PCS-B changes the outcome because the island still contains four synchronous machines and therefore a firm voltage reference. The GFL unit re-locks after 250 ms and takes the steady droop with its 300 MW rating and 5 MWh, while the GFM unit keeps only inertia and transient droop. The nadir falls to 0.161 Hz, 34.3% below B4, the settling point falls to 0.068 Hz, comfortably inside the limit, the GFM converter spends only 3.7% of the window on its current limit, and the GFM SOC ends at 0.495 rather than 0.050. The GFM unit is therefore still available for the next contingency, which is the whole point of reserving it. The one index on which PCS-B is worse is RoCoF, 0.304 Hz/s against 0.269 Hz/s, a 13% penalty that arises because B4 dumps its full limited current in the first cycle while PCS-B splits

the response between two units, one of which is deliberately held back for 250 ms. Both values are far above any realistic RoCoF setting for a 21% deficit, so the comparison that matters in this case is the nadir and the settling point.

6.5 Sensitivity to the Current Limit and to the GFL Delay

Table 10 and Fig. 8 sweep the two parameters that the average-system-frequency model could not represent. When the GFM current limit is lowered from 200 MW to 75 MW, the island nadir under B4 degrades from 0.250 Hz to 0.313 Hz and the proportion of the window spent in limit rises from 33.8% to 99.7%, so at 75 MW the benchmark is saturated for essentially the entire event and its droop law has no authority at all. PCS-B is flat at 0.161 Hz across the same range, and its time in limit stays below 4%, because the bulk of its steady response is carried by the larger GFL unit. The ratio between the two widens from 1.5 to 1.9 as the limit tightens.

Table 10 Sensitivity of the islanded IEEE 39-bus case to the GFM-ES current limit and to the GFL-ES measurement delay

GFM-ES current limit	**75 MW**	**100 MW**	**150 MW**	**200 MW**
B4, nadir (Hz)	0.313	0.291	0.245	0.250
B4, time in current limit (%)	99.7	74.6	49.2	33.8
PCS-B, nadir (Hz)	0.161	0.161	0.161	0.161
PCS-B, time in current limit (%)	3.8	3.8	3.7	3.7
GFL-ES measurement delay	100 ms	200 ms	300 ms	400 ms
B4, nadir (Hz)	0.245	0.245	0.245	0.245
PCS-B, nadir (Hz)	0.161	0.171	0.184	0.195

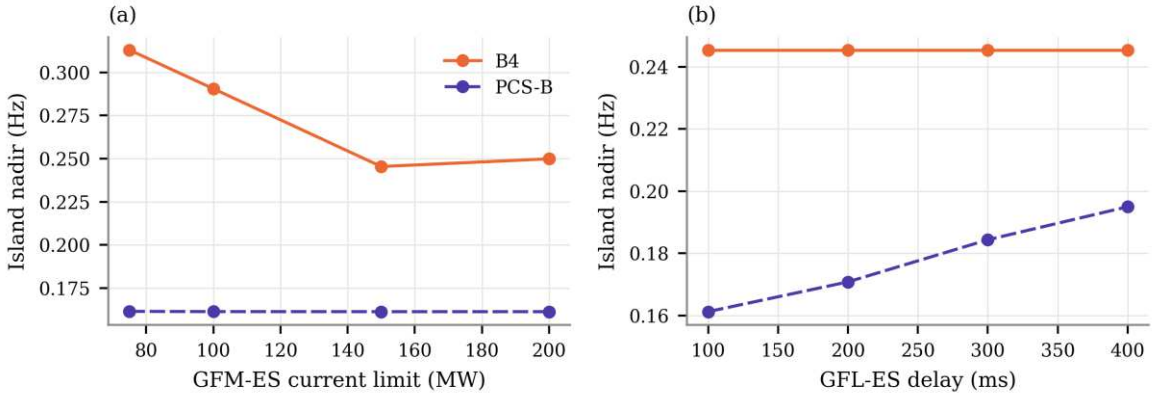


Fig. 8 Sensitivity of the island nadir on the IEEE 39-bus system. a Against the GFM-ES current limit. b Against the GFL-ES measurement delay

The delay sweep is the mirror image. B4 does not use its GFL unit in the island at all, so its nadir is insensitive to the GFL delay at 0.245 Hz. PCS-B does use it, so its nadir degrades from 0.161 Hz at 100 ms to 0.171, 0.184 and 0.195 Hz at 200, 300 and 400 ms. Even at 400 ms it remains 20.5% below the benchmark, and the degradation is gradual rather than abrupt because the predictor of (9) recovers part of the lost phase. This is the honest boundary of the re-lock idea: it trades insensitivity to delay for

a large gain in nadir and in steady-state compliance, and the trade is favourable over the whole range of delays that a wide-area frequency measurement is likely to introduce.

6.6 Discussion and Limitations

Taken together, the two models support two different kinds of claim. In the average-system-frequency study PCS-RG matches the benchmark on SOC and RoCoF and lowers the nadir by 9.6%, but by (7) it cannot also lower the average deviation, and the best achievable largest index ratio was about 1.01. In the 39-bus study the interconnected advantage shrinks to nothing on the nadir and reappears as a 41% reduction in GFM peak power, while the islanded advantage becomes decisive once the converter current limit and the GFM energy are represented. The contribution of this paper is therefore best described as delay robustness, converter duty and islanded frequency security rather than as a uniform improvement in every index.

The study retains limits. The 39-bus model is an RMS electromechanical representation with classical machines and constant impedance loads, so inner converter loops, voltage control and fault behaviour are outside its scope; a full electromagnetic transient study, and hardware-in-the-loop tests, are the natural next step. The current limit is applied to the magnitude of the injected current without a virtual impedance or a priority between the active and reactive components, which is a simplification of the schemes examined in [29]. The re-lock of PCS-B is modelled as a fixed 250 ms outage of the GFL unit rather than as a PLL transient, and the short-circuit ratio condition is checked but not stressed. The RoCoF predictor has been exercised on a washed-out network frequency but not on noisy field measurements. Finally, the storage energies used here are deliberately short so that energy limits appear inside the PFR horizon; they are a stress test, not a sizing recommendation.

7 Conclusion

PCS-RG coordinates grid-forming and grid-following storage for primary frequency regulation without forecasting the nadir. In grid-connected operation the GFM unit supplies virtual inertia and a wash-out droop while the GFL unit acts on a delay-compensated frequency with a front-loaded gain, which keeps the loop linear between events and leaves its delay margin at 0.57 s even with a 22% higher GFL gain. In islanded operation an energy-aware trajectory and an identification-based guard size the GFM droop, and the GFL unit re-locks when synchronous machines remain in the island.

On a three-area average-system-frequency model the nadir was 9.6% lower than a deviation-scheduled benchmark at unchanged state of charge, 33% lower at 300 to 400 ms of GFL delay, and islanded RoCoF fell by 30%, while steady-state violations under parameter and disturbance errors fell from 48% of cases to none. On the IEEE 39-bus system with machine dynamics and converter current limits, the interconnected nadirs of all schemes agreed to within 1% but the proposed scheme required 41% less GFM peak power, and in a 15-bus island with a 548 MW deficit it held a 0.161 Hz nadir and a 0.068 Hz settling point with the GFM state of charge at 0.495, where the benchmark saturated its

converter, exhausted the same unit after 15 s and settled outside the 0.12 Hz limit. The advantage grows as the current limit tightens and persists over GFL delays up to 400 ms.

Declarations

Funding The author declares that no funds, grants or other support were received during the preparation of this manuscript.

Conflict of interest The author declares no competing interests.

Data availability The simulation models, controller code and the scripts that generate every figure and table in this paper are available from the author on reasonable request.

Ethical approval Not applicable. This study involves no human participants or animals.

References

1. Milano F, Dörfler F, Hug G, Hill DJ, Verbič G (2018) Foundations and challenges of low-inertia systems (invited paper). In: 2018 Power Systems Computation Conference (PSCC), Dublin, pp 1-25. https://doi.org/10.23919/PSCC.2018.8450880
2. Tielens P, Van Hertem D (2016) The relevance of inertia in power systems. Renew Sustain Energy Rev 55:999-1009. https://doi.org/10.1016/j.rser.2015.11.016
3. Fang J, Li H, Tang Y, Blaabjerg F (2019) On the inertia of future more-electronics power systems. IEEE J Emerg Sel Top Power Electron 7(4):2130-2146. https://doi.org/10.1109/JESTPE.2018.2877766
4. Anderson PM, Mirheydar M (1990) A low-order system frequency response model. IEEE Trans Power Syst 5(3):720-729. https://doi.org/10.1109/59.65898
5. Ahmadyar AS, Riaz S, Verbič G, Chapman AC, Hill DJ (2018) A framework for assessing renewable integration limits with respect to frequency performance. IEEE Trans Power Syst 33(4):4444-4453. https://doi.org/10.1109/TPWRS.2017.2773091
6. Oudalov A, Chartouni D, Ohler C (2007) Optimizing a battery energy storage system for primary frequency control. IEEE Trans Power Syst 22(3):1259-1266. https://doi.org/10.1109/TPWRS.2007.901459
7. Baek M-K, Roh J-H, Park J-B, Jeong W-C (2022) Optimal sizing of battery/supercapacitor hybrid energy storage systems for frequency regulation. J Electr Eng Technol 17(1):111-120. https://doi.org/10.1007/s42835-021-00867-6
8. Kumar A, Shankar R (2021) A quasi opposition lion optimization algorithm for deregulated AGC considering hybrid energy storage system. J Electr Eng Technol 16(6):2995-3015. https://doi.org/10.1007/s42835-021-00835-0
9. Sun M, Jia Q, Pei Z, Dong C, Wang Z, Jin X (2019) Advanced frequency support strategy of double-stage grid-connected PV generation. J Electr Eng Technol 14(6):2239-2250. https://doi.org/10.1007/s42835-019-00263-1
10. Kerdphol T, Rahman FS, Mitani Y (2018) Virtual inertia control application to enhance frequency stability of interconnected power systems with high renewable energy penetration. Energies 11(4):981. https://doi.org/10.3390/en11040981
11. Rosso R, Wang X, Liserre M, Lu X, Engelken S (2021) Grid-forming converters: control approaches, grid-synchronization, and future trends - a review. IEEE Open J Ind Appl 2:93-109. https://doi.org/10.1109/OJIA.2021.3074028
12. Lasseter RH, Chen Z, Pattabiraman D (2020) Grid-forming inverters: a critical asset for the power grid. IEEE J Emerg Sel Top Power Electron 8(2):925-935. https://doi.org/10.1109/JESTPE.2019.2959271
13. Matevosyan J, Badrzadeh B, Prevost T, Quitmann E, Ramasubramanian D, Urdal H, Achilles S, MacDowell J, Huang SH, Vittal V, O'Sullivan J, Quint R (2019) Grid-forming inverters: are they the key for high renewable penetration? IEEE Power Energy Mag 17(6):89-98. https://doi.org/10.1109/MPE.2019.2933072
14. Shintai T, Miura Y, Ise T (2014) Oscillation damping of a distributed generator using a virtual synchronous generator. IEEE Trans Power Deliv 29(2):668-676. https://doi.org/10.1109/TPWRD.2013.2281359

15. Singh SK, Singh R, Ashfaq H, Sharma SK (2023) Virtual synchronous machine using ant colony optimization in inverter interfaced distributed generation (IIDG). J Electr Eng Technol 18(1):167-179. https://doi.org/10.1007/s42835-022-01198-w

16. Yan J, Qin F (2025) Adaptive virtual inertia strategy for grid-forming inverters based on Andronov-Hopf oscillator control. J Electr Eng Technol 21(1):559-572. https://doi.org/10.1007/s42835-025-02399-9

17. Sun J, Cai W, Guo Q, Li Y (2025) Enhanced transient stability control strategy for VSG taking into account fault current and grid-forming capability. J Electr Eng Technol 21(2):1671-1687. https://doi.org/10.1007/s42835-025-02500-2

18. Kang Z, Li L, Dong Z (2024) Research on nonlinear robust control strategy of active voltage support for grid-forming photovoltaics. J Electr Eng Technol 20(3):1321-1331. https://doi.org/10.1007/s42835-024-02087-0

19. Zhu Z, Sun S, Li Z, Huang S (2024) Impedance modeling and stability mechanism analysis for grid forming and grid following converters. J Electr Eng Technol 19(5):2973-2985. https://doi.org/10.1007/s42835-024-01814-x

20. Wang X, Taul MG, Wu H, Liao Y, Blaabjerg F, Harnefors L (2020) Grid-synchronization stability of converter-based resources - an overview. IEEE Open J Ind Appl 1:115-134. https://doi.org/10.1109/OJIA.2020.3020392

21. Lu X, Sun K, Guerrero JM, Vasquez JC, Huang L (2014) State-of-charge balance using adaptive droop control for distributed energy storage systems in DC microgrid applications. IEEE Trans Ind Electron 61(6):2804-2815. https://doi.org/10.1109/TIE.2013.2279374

22. Chang X, Li R, Wang Y, Zhai M, Cai J (2024) A two-stage SOC balancing control strategy for distributed energy storage systems in DC microgrids based on improved droop control. J Electr Eng Technol 19(7):3891-3905. https://doi.org/10.1007/s42835-024-01835-6

23. Jiang L, Yao W, Wu QH, Wen JY, Cheng SJ (2012) Delay-dependent stability for load frequency control with constant and time-varying delays. IEEE Trans Power Syst 27(2):932-941. https://doi.org/10.1109/TPWRS.2011.2172821

24. Wall P, Terzija V (2014) Simultaneous estimation of the time of disturbance and inertia in power systems. IEEE Trans Power Deliv 29(4):2018-2031. https://doi.org/10.1109/TPWRD.2014.2306062

25. Reddy ChR, Reddy KH, Aymen F, Goud BS, Bajaj M, Abdulaal MJ, Milyani AH (2022) Hybrid ROCOF relay for islanding detection. J Electr Eng Technol 17(1):51-60. https://doi.org/10.1007/s42835-021-00856-9

26. Storn R, Price K (1997) Differential evolution: a simple and efficient heuristic for global optimization over continuous spaces. J Glob Optim 11(4):341-359. https://doi.org/10.1023/A:1008202821328

27. Athay T, Podmore R, Virmani S (1979) A practical method for the direct analysis of transient stability. IEEE Trans Power Appar Syst PAS-98(2):573-584. https://doi.org/10.1109/TPAS.1979.319407

28. Zimmerman RD, Murillo-Sanchez CE, Thomas RJ (2011) MATPOWER: steady-state operations, planning, and analysis tools for power systems research and education. IEEE Trans Power Syst 26(1):12-19. https://doi.org/10.1109/TPWRS.2010.2051168

29. Qoria T, Gruson F, Colas F, Denis G, Prevost T, Guillaud X (2020) Critical clearing time determination and enhancement of grid-forming converters embedding virtual impedance as current limitation algorithm. IEEE J Emerg Sel Top Power Electron 8(2):1050-1061. https://doi.org/10.1109/JESTPE.2019.2959085